# Figure S1

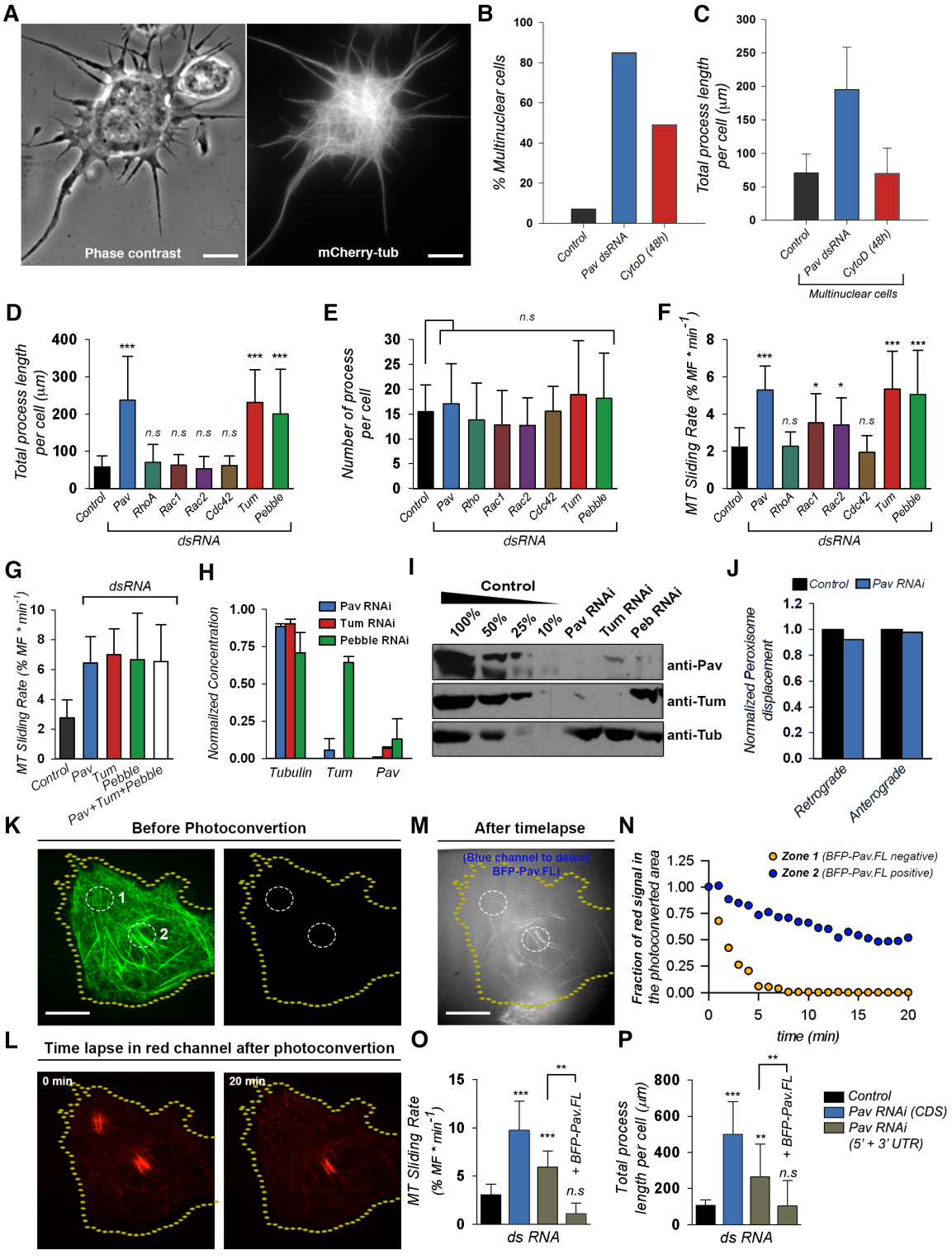
A
Phase contrast
mCherry-tub
B
% Multinuclear cells
Control
Pav dsRNA
CytoD (48h)
C
Total process length per cell (µm)
Control
Pav dsRNA
CytoD (48h)
Multinuclear cells
D
Total process length per cell (µm)
Control
Pav
RhoA
Rac1
Rac2
Cdc42
Tum
Pebble
dsRNA
E
Number of process per cell
n.s
Control
Pav
Rho
Rac1
Rac2
Cdc42
Tum
Pebble
dsRNA
F
MT Sliding Rate (% MF * min-1)
Control
Pav
RhoA
Rac1
Rac2
Cdc42
Tum
Pebble
dsRNA
G
MT Sliding Rate (% MF * min-1)
dsRNA
Control
Pav
Tum
Pebble
Pav+Tum+Pebble
H
Normalized Concentration
Pav RNAi
Tum RNAi
Pebble RNAi
Tubulin
Tum
Pav
I
Control
100%
50%
25%
10%
Pav RNAi
Tum RNAi
Peb RNAi
anti-Pav
anti-Tum
anti-Tub
J
Control
Pav RNAi
Normalized Peroxisome displacement
Retrograde
Anterograde
K
Before Photoconvertion
1
2
M
After timelapse
(Blue channel to detect BFP-Pav.FL)
N
Zone 1 (BFP-Pav.FL negative)
Zone 2 (BFP-Pav.FL positive)
Fraction of red signal in the photoconverted area
time (min)
L
Time lapse in red channel after photoconvertion
0 min
20 min
O
MT Sliding Rate (% MF * min-1)
+ BFP-Pav.FL
ds RNA
P
Total process length per cell (µm)
+ BFP-Pav.FL
ds RNA
Control
Pav RNAi (CDS)
Pav RNAi (5' + 3' UTR)

**Figure S1. Pav-KLP regulates microtubule sliding and process formation independently of small Rho GTPases in S2 cells.** Related to Figure 1.

(A) CytoD treatment induced microtubule-filled processes in *Drosophila* S2. Scale bar, 5 $\mu$m.

(B and C) Polyploid cells induced by long treatment of CytoD did not develop longer processes than control cells. (B) Treatment of Pav-KLP dsRNA induced formation of multinuclear cells due to cytokinesis impairment. Alternatively, the number of S2 polynuclear cells could be increased by long treatment of the actin-fragmentation drug CytoD. (n>100 cells for each category.) (C) Quantification of process length in mononuclear (control) and multinuclear cells treated with either Pav-KLP dsRNA or CytoD. (n>80 cells for each catergory; error bars, SD).

(D-G) Depletion of Centralspindlin complex components activated microtubule sliding and process formation independently of small Rho GTPases in S2 cells. Process length (D) and number of processes (E) were quantified per cell after knockdown of Centralspindlin components or small Rho GTPases family proteins. (n>70 cells for each catergory; error bars, SD) ***, $p < 0.0005$, unpaired t test. (F) Quantification of microtubule sliding in S2 cells treated with dsRNA. (n>10 cells for each catergory; error bars, SD) ***, $p < 0.0005$; *, $p= 0.045$. (G) Simultaneous treatment of Pav-KLP, Tumbleweed and Pebble dsRNA does not have an additive effect on microtubule sliding activation. (n>15 cells for each catergory; error bars, SD).

(H-I) Pav-KLP stability was diminished when Tumbleweed or Pebble are depleted by dsRNA. (H) Protein levels were quantified after western blot in two independent experiments.(I) Representative western blots of the S2 lysates described in (H). Dilutions of untreated cells provided to estimate degree of knockdown.

(J) Quantification of peroxisome transport in S2 cells. Peroxisomes located in the S2 processes were tracked for 1 minute, and retrograde and anterograde run-trajectories for each peroxisome were determined by DiaTracker (Semasopht). Peroxisome displacement was normalized to the untreated control (n>663 peroxisomes from 25 cells for each condition).

(K-N) Ectopic expression of BFP-Pav.FL blocked microtubule sliding. An S2 cell coexpressing tdEOS-αtub and BFP-Pav.FL was photoconverted in two different areas and microtubule sliding was quantified. (K) Confocal images of green and red channel before photoconversion. Scale bar, 10 $\mu$m. (L) The first and last frame (20 minutes) of a

time-lapse in the red channel are depicted. Note that photoconverted microtubules in zone 2 were static. See movie S2. (M) After the time-lapse acquisition, BFP-Pav.FL localization was detected with blue light. Note that Pav-KLP decorated Microtubules were static while microtubules in the other zone without Pav-KLP moved freely. Scale bar, 10 $\mu$m. (N) Quantification of the relative red signal remaining in the photoconverted zone.

(O-P) Expression of the Pav-KLP full length protein rescues sliding rates and process formation. Quantification of microtubule sliding (O) and process formation (P) in S2 cells treated with dual dsRNAs against the Pav-KLP 5' and 3' UTR sequences. BFP-Pav.FL rescued both sliding and process formation. ***, $p < 0.001$; **,$p > 0.0025$ ($n>10$ cells for each category; error bars, SD).

# Figure S2

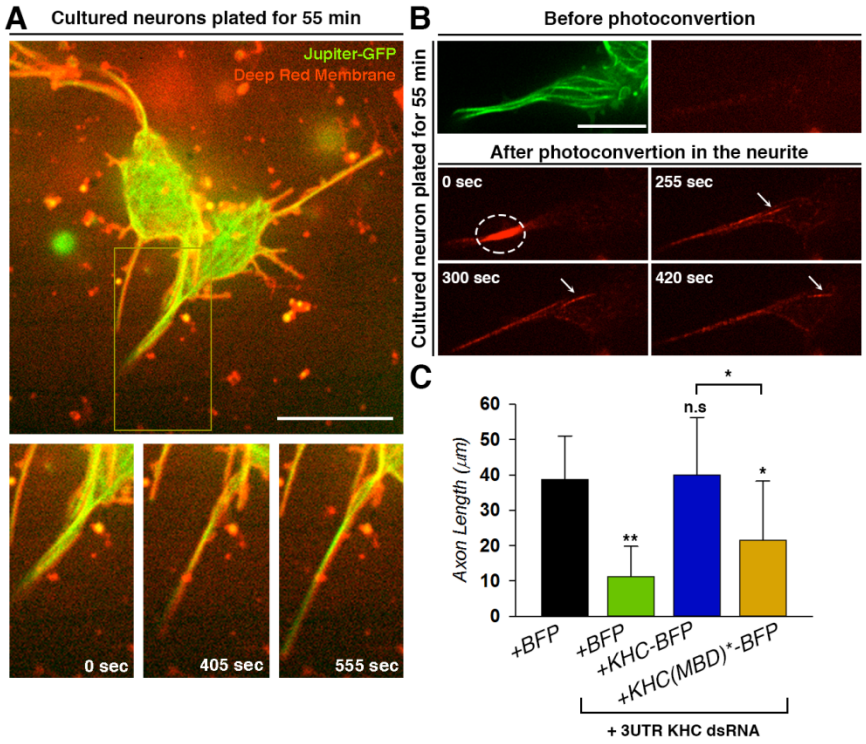


**Figure S2. Microtubule sliding drives neurite outgrowth in young neurons.** Related to Figure 2.

(A) A confocal image of young cultured neurons expressing endogenous GFP-tagged Jupiter with the plasma membrane stained with Deep Red (upper panel). Time-lapse acquisition showed that neurite outgrowth is coupled to microtubule motility (bottom panels). See movie S3. Scale bar, 5 μm.

(B) Microtubules slide as long fragments in young *Drosophila* neurons. The arrows track the movement of a long microtubule after photoconversion in the neurite of a young neuron expressing *mat αtub*>tdEOS-αtub. See movie S3. Scale bar, 5 μm.

(C) Kinesin-1 drives axon outgrowth in *Drosophila* neurons. Depletion of KHC by zygotic protein null ($khc^{27}$) and injection of dsRNA against the 3'UTR of KHC resulted in neurons with very short neurites. Coinjection of pMT-KHC-BFP, but not of pMT-KHC(MBD)*-BFP, rescued the length of the axons. The mean and SD are shown (n>10 neurons per category; **p= 0.0019, and *p>0.0425, unpaired t test).

# Figure S3

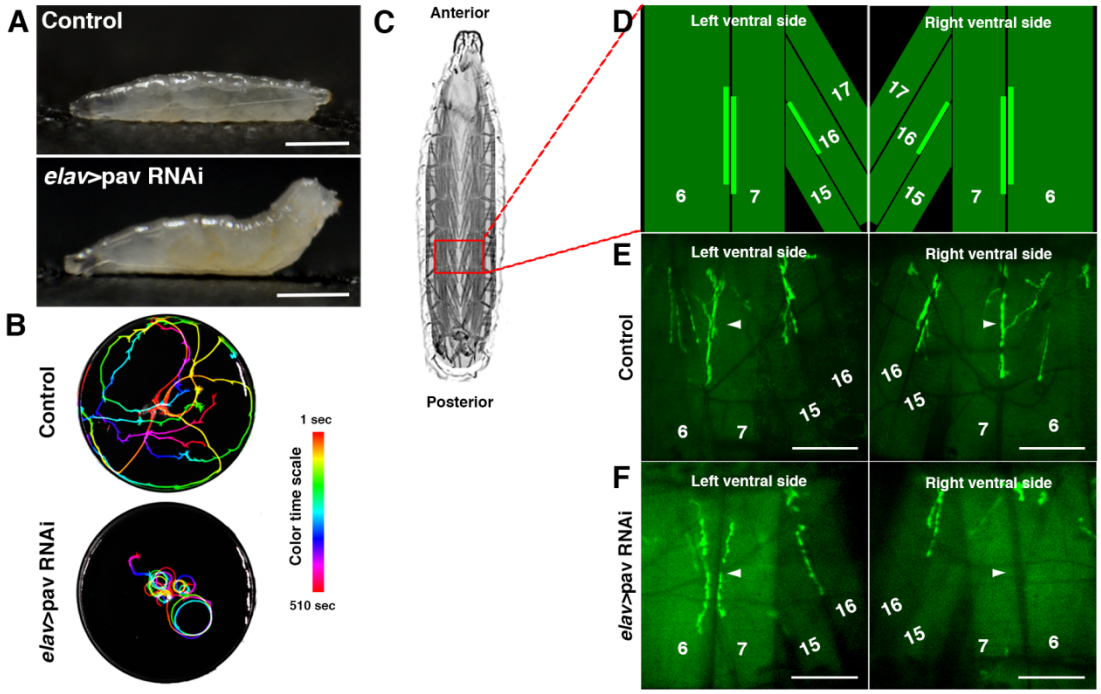


**Figure S3. Pav-KLP regulates neuromuscular junction formation.** Related to Figure 4.

(A) When crawling, wild type third instar larvae maintained a flat body posture. In contrast, most *elav>pav* RNAi larvae exhibited a posterior paralysis and a classical tail-flipping phenotype indicating a defect in proper motor neuron development. Scale bar, 1 mm.

(B) Third instar larvae expressing *elav>pav* RNAi have severe locomotion defects. Crawling trajectories of surviving larvae were represented as multicolor merge images using the Temporal-Color Code plugin in Fiji (n=7 larvae per condition). See corresponding Movie S5.

(C) Cartoon representing a ventral view section of the third instar larval musculature. The segment used to analyse NMJs is highlighted with the red rectangle.

(D) Schematic diagrams of NMJs on ventral muscles 6/7 of a wild-type larva. The muscles and NMJs are highlighted with dark and light green, respectively.

(E and F) Some neuromuscular terminals are missing in *elav>pav* RNAi knockdown third instar larvae. Confocal images (Z-projections, maximal intensity) of NMJs labeled by

MHC-CD8-GFP-SH in segment A6 of control (E) and *elav>pav* RNAi (F) intact third instar larvae. Arrowheads indicate the NMJs that innervate muscles 6 and 7. Note that this NMJ is missing in the right hemisegment of the *elav>pav* RNAi larva. Scale bars, 100 $\mu$m.

## Supplemental experimental procedures

### Cell Culture and RNAi

*Drosophila* S2 cells were cultured as previously described [S1]. For knockdown experiments, cultures at 1.5 x$10^6$ cells/mL were treated twice with 20 $\mu$g of dsRNA (day 1 and 3) and cell analysis performed on day 5. Primers used in PCR reactions to create T7 templates from genomic DNA are described below. Culture of *Drosophila* neurons was dissociated from gastrulation embryos as previously described [S2]. To reduce maternal load of Pav-KLP, embryos at the blastoderm stage were microinjected with Pav-KLP dsRNA (three different positions for each embryo) supplemented with Cascade blue dextran as a tracer dye as previously described [S3].

### Plasmids and cloning

To visualize Pav-KLP in S2 cells, a plasmid encoding Full Length Pav-KLP cDNA (gift from E. Griffis) was cloned into the pMT-GFP backbone by EcoRI-NotI restriction enzyme sites to generate GFP-Pav.FL. GFP-Pav.NLS(4-7)* (replacement of the $K_{770}$NR and $R_{843}$KR by AAA) and GFP-Pav.DEAD (G131E) were created by PCR amplification using the primers described in [S4]. To generate GFP-Pav.Stalk nucleotides corresponding to amino acids 503-710 of Pav-KLP were amplified using the oligonucleotides GCCGGAATTCTACAGTTTGGGACCCGATTTTCC and GCGCGCGGCCGCTTACGTATATGCACCGCGATCTTTC, and the PCR product was cloned into pMT-GFP by EcoRI-NotI. For photoconversion experiments the same Pav-KLP DNA fragments were inserted into the pMT-BFP (pMT-BFP was generated by inserting mTagBFP2, gift of V. Verkhusha, into pMT by KpnI and EcoRI) by EcoRI-NotI to generate BFP-Pav.FL, BFP-Pav.NLS(4-7)*, BFP-Pav.DEAD and BFP-Pav.Stalk. To visualize microtubules, a tandem-dimer (td) of EOS2 or mCherry was tagged to

αTub84B to create pMT-tdEOS-αtub [S1] and pMT-mCherry-tub [S5]. KHC(MBD)* was created by the substitution of $R_{914}$KRYQ to AAAYA in the KHC cDNA. Then KHC and KHC(MBD)* were cloned into pAC-BFP backbone to create pAC-KHC-BFP and pAC-KHC(MBD)*-BFP. Plasmid encoding pAC-GFP-SKL was previously used to visualize peroxisome movement [S6].

**Fly Stocks and Genetics**

Fly stocks were maintained on standard cornmeal food at 25 °C incubator. Following fly stocks were obtained from the Bloomington stock center: *pav$^{B200}$* (Stock #4384), *pav-RNAi TRiP Valium$^{20}$* (Stock #42573), *maternal αTub67C-Gal4* (Stock #7062 and #7063), and *Dr$^{Mio}$/TM3, twist-GFP* (stock #6663). Two endogenous protein trap lines, Jupiter-GFP (ZCL2183) and Nrv2-GFP (ZCL2903), were obtained from Yale FlyTrap database. Other fly stocks were generous gifts from the following labs: *UASp-GFP-Pav.NLS(4-7)* ,* D. Glover lab [S7]; *pros-Gal4,*and *elav-Gal4*, C. Doe lab [S8]; *UASp-GFP*, and *yw; wg$^{Sp-1}$/CyO; Dr$^{Mio}$/TM3, Sb*, E. Ferguson lab [S9]; *MHC-CD8-GFP-SH*, B. McCabe lab [S10]. UASp- tdEOS-αtub transgenic lines were previously made in our lab [S3] and now available in Bloomington stock center (Stock #51313 and #51314).

In order to screen *pav$^{B200}$* zygotic homozygote in live embryos and live neuronal culture, we crossed males of *yw; P{lacW}64A pav$^{B200}$ Diap$^{11}$ st$^{1}$ cu$^{1}$ sr$^{1}$ e$^{s}$ ca$^{1}$/TM6B, P{iab-2(1.7)lacZ}6B, Tb* (Bloomington Stock #4384) with females of *w; Dr$^{Mio}$/TM3, P{GAL4-twi.G}2.3, P{UAS-2xEGFP}AH2.3, Sb Ser* (Bloomington Stock #6663) to establish the stock of *w; P{lacW}64A pav$^{B200}$ Diap$^{11}$ st$^{1}$ cu$^{1}$ sr$^{1}$ e$^{s}$ ca$^{1}$/ TM3, P{GAL4-twi.G}2.3, P{UAS-2xEGFP}AH2.3, Sb Ser* (for short, *w; pav$^{B200}$/TM3, twist-GFP*). Embryos for neuron preparation were collected from the stock of *w; pav$^{B200}$/TM3, twist-GFP* and screened for GFP-negative *pav$^{B200}$* zygotic homozygous embryos. In some experiments to further knock down Pav maternal load, we performed Pav-KLP dsRNA microinjection into

syncytial blastoderm stage of embryos from *w; pav$^{B200}$/TM3, twist-GFP* stock before we screened for the GFP-negative *pav$^{B200}$* zygotic homozygous embryos at gastrulation stage.

In order to ectopically express Pav.NLS(4-7)* mutant in early neurons, embryos for neuron preparation were collected from the cross of females of *w; P{pros-Gal4}* with males of *w; P{UASp-GFP-Pav.NLS(4-7)*}*; embryos were collected from the cross of females of *w; P{pros-Gal4}* with males of *w; P{UASp-GFP}* as a control.

In order to assay microtubule sliding in control young neurons, embryos for neuron preparation were collected from the cross of females of *w; P{maternal αTub67C-Gal4}* with males of *w; P{UASp*-tdEOS-*αTub}*. In order to assay microtubule sliding in *pav$^{B200}$* mutant young neurons, first females of *w; P{UASp-tdEOS-αTub}; Dr$^{Mio}$/TM3, twist-GFP* were crossed with males of *w; P{maternal α-Tub67C-Gal4}; pav$^{B200}$/TM3* to get females of *w; P{UASp-tdEOS-αTub}/P{maternal αTub67C-Gal4}; pav$^{B200}$/TM3, twist-GFP*. These females were then crossed with males of *w; pav$^{B200}$/TM3, twist-GFP* and the embryos from this cross were microinjected with Pav-KLP dsRNA (three sites in each embryo: anterior, middle and posterior) at syncytial blastoderm stage to knock down *pav* maternal-loaded mRNA before neuron preparation.

In order to determine the Pav function in neurons, females of *w; P{elav-Gal4}* were crossed with males of *yv; P{Pav-TRiP-Valium20} attP40*, and the third instar larvae were collected from that cross and washed in 1X PBS before locomotion analysis. In order to examine NMJs in *pav* knockdown flies, females of *yv; P{Pav-TRiP-Valium20} attP40* were crossed with males of *w; P{MHC-CD8-GFP-SH}; P{elav-Gal4}.* The third instar larvae were collected from that cross, and washed in 1X PBS before fixation in 4% formaldehyde for 30 min. The fixed larvae were then mounted between glass slides and coverslips (spaced by two layers of tapes) and imaged on microscope immediately. In

order to examine the motor neuron axon length in *pav* knockdown flies, females of *yw; P{Pav-TRiP-Valium20} attP40; pav$^{B200}$/TM3 were crossed with* males of *yw; Nrv2-GFP; P{elav-Gal4}.* The early second instar larvae were collected from the cross, and washed in $dH_2O$ before anesthetized in 100% EtOH for 1 min.

In order to test the role of C-terminal microtubule binding domain of KHC in neurite development, four groups of embryos were collected and injected with DNA and/or RNA (at three sites each embryo: anterior, middle, posterior) at blastoderm stage before cellularization: 1) embryos from the stock *w$^{1118}$* were injected with pAC-tdEOS-αtub and pAC-BFP; 2) embryos from the stock *Khc$^{27}$/CyO, twist-GFP* were injected with pAC-tdEOS-αtub, pAC-BFP and dsRNA against Khc 3'-UTR; 3) embryos from the stock *Khc$^{27}$/CyO, twist-GFP* were injected with pAC-tdEOS-αtub, pAC-KHC1-975 FL-BFP and dsRNA against Khc 3'-UTR; 4) embryos from the stock *Khc$^{27}$/CyO, twist-GFP* were injected with pAC-tdEOS-αtub, pAC-KHC(MBD)*-BFP and dsRNA against Khc 3'-UTR. These injected embryos were left in a moisture chamber at 25°C to develop for another 4-5 h before neuron preparation.

**Microscopy and image acquisition**

To image microtubule sliding in *Drosophila* S2 and primary neurons, a Nikon Eclipse U2000 inverted microscope equipped with a Yokogawa CSU10 spinning disc head, Perfect Focus system (Nikon) and a 100 X 1.45 NA lens was used. Images were acquired using Evolve EMCCD (Photometrics) and controlled by Nikon Elements software. Photoconversion of *tdEOS-αtub* was performed using illumination from a heliophore laser (405 nm) in the epifluorescence pathway and confined in the field diaphragm position either by a slit (*Drosophila* S2 cells) or adjustable diaphragm (*Drosophila* neurons). Images were collected once per minute for 20 min (S2 cells) or each 15 sec for 2 or 10 min (cultured neurons). To image NMJs in whole larvae, multiple

z sections were collected on the confocal microscope and images were projected (maximal intensity). To visualize processes and peroxisome transport in S2 cells or nervous system in early second larvae, images were acquired on a Nikon Eclipse U2000 inverted microscope equipped with Plan-Apo 100x (for S2 cells) or 10x (for larvae) 1.4 NA objective and a CoolSnap ES CCD camera (Roper Scientific), controlled by MetaMorph software (Version 7.7.5.0, Molecular Devices). To measure axon lengths of live neurons, phase-contrast images were obtained using a 100 W halogen lamp, and fluorescence excitation was achieved using an Aura light engine (Lumencor). Quantification of organelle transport was performed as previously described [S2]. Quantification of the process length in S2 cells was automatically performed using a custom FIJI routine. Quantification of the axon length of segmental nerves of the *Drosophila* larvae was performed manually. All images were analyzed in FIJI, chart diagrams were created in SigmaPlot, and all figures and movies were assembled in Photoshop and FIJI, respectively.

**Analysis of Microtubule Sliding**

To calculate the rate of microtubule sliding, each frame of a time-lapse sequence was converted to a binary image using the IsoData Autothreshold Plug-In of Fiji. The fraction of the photoconverted microtubules moving outside of the initial photoconverted area for each frame ($MFi$) was calculated as following:

$$MFi = \frac{(Oi - O1)}{(Ti - O1)}$$

where $Oi$ and $Ti$ are the intensities of photoconverted microtubules measured outside of the original photoconverted area and the whole cell for each frame, respectively. While $O1$ is the intensity measured outside of the photoconverted area at the first frame. As microtubules move outside of the initial photoconversion area, this ratio increases. The

rate of the increase is nearly constant for times t < 10 min; this number was taken as the rate of sliding (%MF * $min^{-1}$). Statistical significance was determined using a two-tailed Student's t-test, with a confidence interval of 95%

**Antibodies and immunostaining**

For western blot analysis of S2 cell extracts, the following primary antibodies were used: rabbit anti-Pav-KLP (gift from J. Scholey lab) [S11]; rat anti-Tumbleweed (gift from M. Murray) [S12]; mouse anti-Dm1α (Sigma). For immunostaining, S2 cells were fixed with methanol and blocked and washed with wash buffer (TBS buffer supplemented with 1% BSA and 0.1% Triton X-100). Microtubules and nuclei were staining using Dm1α (1:1000) and DAPI (0.6 mg/l), respectively.

**Assays with *Drosophila* larvae**

Larvae were allowed to crawl on the surface of 2% agarose containing apple juice and commercial charcoal powder to increase the contrast between the larvae and the background. Trajectories of larvae displacement were represented as multicolor merge images using the Temporal-Color Code plugin in Fiji.

**Primers used for dsRNA synthesis**

| Gene | Primer 1 (5' - 3') | Primer 2 (5' - 3') |
|---|---|---|
| Pav-KLP CDS | AAATCCGTAACGAAACTAACCG | ACAACTGCTCTTGGCAGATACC |
| Pav-KLP 5'UTR | TCGGTCACTCTAAAACCAAGCGTG | GTTGTCAGCTCGTTTTTGCAACTAA |
| Pav-KLP 3'UTR | AAATGACTCAGCGTGGAATTCTC | CAGTATATGCGCGTAATTCACTTTAT |
| Tumbleweed | TTGCGCATGTTCGAGCAGTACCACG | TCCGACAGCAACGATCCGGTGG |
| Pebble | GATGGACTATCTGTTTGGCGACTATTTGGATAGCAT | CGACTTATTAAGCAGCGGATCATTGGTTTCAGC |
| RhoA | AGGTGGAGCTGGCCTTGTGGGATAC | AGCGAATCGGGTGAATCCACTGAGAAAC |
| Rac1 | ACCATGCAGGCGATCAAGTGCGTC | ATGCCGGATTCACCAGCGAGAAGC |
| Rac2 | ACCAGTACAGTAGCCTTCATCATGCAGG | TCTCAAACGATGCCGGATTCACCAGTG |
| CDC42 | AGGCCGTCAAGTACGTGGAGTGCTC | GACACTACTGACACAGATACGCGG |

T7 promoter sequences (TAATACGACTCACTATAGGG) were added to 5' end of each primer.

**Supplemental References**


S1. Barlan, K., Lu, W., and Gelfand, V.I. (2013). The microtubule-binding protein ensconsin is an essential cofactor of Kinesin-1. Curr Biol *23*, 317-322.

S2. Lu, W., Del Castillo, U., and Gelfand, V.I. (2013). Organelle transport in cultured *Drosophila* cells: S2 cell line and primary neurons. J Vis Exp, e50838.

S3. Lu, W., Fox, P., Lakonishok, M., Davidson, M.W., and Gelfand, V.I. (2013). Initial neurite outgrowth in *Drosophila* neurons is driven by Kinesin-powered microtubule sliding. Curr Biol *23*, 1018-1023.

S4. Minestrini, G., Mathe, E., and Glover, D.M. (2002). Domains of the Pavarotti kinesin-like protein that direct its subcellular distribution: effects of mislocalisation on the tubulin and actin cytoskeleton during *Drosophila* oogenesis. J Cell Sci *115*, 725-736.

S5. Jolly, A.L., Kim, H., Srinivasan, D., Lakonishok, M., Larson, A.G., and Gelfand, V.I. (2010). Kinesin-1 heavy chain mediates microtubule sliding to drive changes in cell shape. Proc Natl Acad Sci U S A *107*, 12151-12156.

S6. Wiemer, E.A., Wenzel, T., Deerinck, T.J., Ellisman, M.H., and Subramani, S. (1997). Visualization of the peroxisomal compartment in living mammalian cells: dynamic behavior and association with microtubules. J Cell Biol *136*, 71-80.

S7. Minestrini, G., Harley, A.S., and Glover, D.M. (2003). Localization of Pavarotti-KLP in living *Drosophila* embryos suggests roles in reorganizing the cortical cytoskeleton during the mitotic cycle. Mol Biol Cell *14*, 4028-4038.

S8. Pearson, B.J., and Doe, C.Q. (2003). Regulation of neuroblast competence in *Drosophila*. Nature *425*, 624-628.

S9. Lu, W., Casanueva, M.O., Mahowald, A.P., Kato, M., Lauterbach, D., and Ferguson, E.L. (2012). Niche-associated activation of rac promotes the asymmetric division of *Drosophila* female germline stem cells. PLoS Biol *10*, e1001357.

S10. McCabe, B.D., Hom, S., Aberle, H., Fetter, R.D., Marques, G., Haerry, T.E., Wan, H., O'Connor, M.B., Goodman, C.S., and Haghighi, A.P. (2004). Highwire regulates presynaptic BMP signaling essential for synaptic growth. Neuron *41*, 891-905.

S11. Sommi, P., Ananthakrishnan, R., Cheerambathur, D.K., Kwon, M., Morales-Mulia, S., Brust-Mascher, I., and Mogilner, A. (2010). A mitotic kinesin-6, Pav-KLP, mediates interdependent cortical reorganization and spindle dynamics in *Drosophila* embryos. J Cell Sci *123*, 1862-1872.

S12. Somers, W.G., and Saint, R. (2003). A RhoGEF and Rho family GTPase-activating protein complex links the contractile ring to cortical microtubules at the onset of cytokinesis. Dev Cell *4*, 29-39.